1-1-2015

A semi-analytical analysis of the stability of the reversible Selkov model

Khaled. Al Noufaey
University of Wollongong, ksnan708@uowmail.edu.au

Timothy R. Marchant
University of Wollongong, tim@uow.edu.au

Maureen P. Edwards
University of Wollongong, maureen@uow.edu.au

A semi-analytical analysis of the stability of the reversible Selkov model

Abstract

Semi-analytical solutions for the reversible Selkov model are developed and used to investigate its static and dynamic stability. A one-dimensional reaction-diffusion cell is considered with all steps of the Selkov reaction modeled. A coupled set of four partial differential equations is obtained for the precursor, reactant, autocatalyst and final product concentrations. The Galerkin method is applied to approximate the spatial structure of the concentrations to obtain a lower-order, ordinary differential equation model, as an approximation to the governing partial differential equations. The semi-analytical model is analysed to obtain steady-state solutions, bifurcation diagrams and parameter maps in which the different types of bifurcation patterns and Hopf bifurcations occur. The results for this model are compared to the standard (two species) Selkov model. The effect of varying the rate constants, associated with the decay of both the precursor and final product, on the stability of the system is considered in detail. It is shown that increasing these rate constants, and hence the coupling between the reactant/autocatalyst and precursor/final product, stabilizes the system by reducing the area of parameter space in which Hopf bifurcations can occur. The effect of feedback, by varying the various concentrations in the boundary reservoirs, in response to the concentrations in the cell, is also considered. Feedback can be either stabilizing or destabilizing, depending on the sign of the feedback response. The semi-analytical method is shown to generate accurate solutions, by comparison with numerical solutions of the governing partial differential equations.

Keywords

selkov, reversible, stability, model, analysis, semi, analytical

Disciplines

Engineering | Science and Technology Studies

Publication Details

Al Noufaey, K., Marchant, T. R. & Edwards, M. P. (2015). A semi-analytical analysis of the stability of the reversible Selkov model. Dynamics of Continuous, Discrete and Impulsive Systems Series B: Applications and Algorithms, 22 (2), 117-139.

A semi-analytical analysis of the stability of the reversible Selkov model

K.S. Al Noufaey, T. R. Marchant and M. P. Edwards

School of Mathematics and Applied Statistics
The University of Wollongong, Wollongong, 2522, N.S.W., Australia.

Abstract. Semi-analytical solutions for the reversible Selkov model are developed and used to investigate its static and dynamic stability. A one-dimensional reaction-diffusion cell is considered with all steps of the Selokov reaction modeled. A coupled set of four partial differential equations is obtained for the precursor, reactant, autocatalyst and final product concentrations. The Galerkin method is applied to approximate the spatial structure of the concentrations to obtain a lower-order, ordinary differential equation model, as an approximation to the governing partial differential equations. The semi-analytical model is analyzed to obtain steady-state solutions, bifurcation diagrams and parameter maps in which the different types of bifurcation patterns and Hopf bifurcations occur. The effect of varying the rate constants, associated with the decay of both the precursor and final product, on the stability of the system is considered in detail. It is shown that increasing these rate constants stabilizes the system by reducing the area of parameter space in which Hopf bifurcations can occur. The effect of feedback, by varying the various concentrations in the boundary reservoirs, in response to the concentrations in the cell, is also considered. Feedback can be either stabilizing or destabilizing, depending on the sign of the feedback response. The semi-analytical method is shown to generate accurate solutions, by comparison with numerical solutions of the governing partial differential equations.

Keywords. reaction-diffusion equations, reversible Selkov model, singularity theory, Hopf bifurcations, semi-analytical solutions, feedback control.

AMS (MOS) subject classification: 35, 37, 41

1 Introduction

Chemical and biological systems can exhibit oscillatory solutions, multiple steady-state solutions and chaotic behaviours which have been of great interest to both theoreticians and experimentalists for many decades. Some experimental examples of oscillatory behaviour in chemical systems include the Bray-Liebhafsky, Belousov-Zhabotinsky and Briggs-Rausher reactions, for which periodic variations in concentrations can be visualized via changes in colour; see [4] for a review of these reactions and other oscillatory phenomena. Biochemical systems are responsible for many of the oscillations associated with cellular processes such as glycolytic oscillations in yeast, calcium ion waves and circadian rhythms, see [7]. A very common reactor scenario, for the investigation of chemical systems, is the continuous flow well-stirred tank reactor (CSTR). Usually, a system of ordinary differential equations (odes) governs a CSTR, which can be analyzed by standard techniques. However the reaction-diffusion cell is also an important reactor scenario, which is governed by a system of partial differential equations (pdes), and is not so easily analyzed by standard combustion theory.

The reversible Selkov model, see [6, 18, 19], is

$$\begin{aligned} A &\rightleftharpoons S, \\ S + 2P &\rightleftharpoons 3P, \\ P &\rightleftharpoons B. \end{aligned} \tag{1}$$

The reactant S corresponds to adenosine triphosphate (ATP) while the autocatalyst P corresponds to adenosine diphosphate (ADP). ATP is a high energy molecule, with three phosphate groups, which is used by the cell to produce and store energy, while ADP is a low-energy molecule with two phosphate groups. A is the precursor and B is the final product. Glucose or fructose are examples of the source inputs into this system.

[18] analyzed a simple ode model system for oscillatory reactions, which included the reversible Selkov reaction (1) in a CSTR. Two kinds of steady-state bifurcation diagrams occur, the unique and the breaking-wave patterns. Also, they found the region where Hopf bifurcations occur and discussed their stability. [6] presented a symmetry-breaking instability for (1). The author found that the time periodic oscillations of the homogeneous model are subject to a symmetry-breaking instability, via Hopf-bifurcation, by coupling with molecular diffusion in a distributed system. This instability generates sinusoidal heterogeneous waves of small wavelengths.

[1] considered semi-analytical solutions for the reversible Selkov model (1). They assumed that the rate constants associated with the forward step of the first reaction, $A \rightarrow S$ (decay of the precursor) and the backwards step of the third reaction $P \leftarrow B$ (decay of the final product) were both very small. They found the steady state solutions and the region of parameter space, in which Hopf bifurcations occur. Also, they examined the effect of feedback strength and delay response on the parameter region in which oscillatory solutions occur.

The Gray & Scott cubic autocatalytic model has been widely studied and [12] considered semi-analytical solutions for the model in a reaction-diffusion cell. The governing pde model was approximated by a lower-order ode model, using the Galerkin method of averaging. The ode model was analyzed using various techniques from combustion theory which allowed bifurcation diagrams and Hopf bifurcation parameter maps to be found. An excellent comparison between the results of the semi-analytical method and the numerical solutions of the governing pdes was found. The Galerkin averaging method has been applied to various other problems such as heat and mass transfer in a porous catalytic pellet [14], feedback control for microwave heating [11] and extensions to the Gray-Scott model such as Michaelis-Menten decay [13].

Feedback control can be applied to alter the stability of a dynamical system. Desirable outcomes from the control algorithm include stabilizing steady states and eliminating limit cycle solutions. It is also possible to create new complex behaviours. [5] considered the chlorine dioxide-iodine reaction in a CSTR, both numerically and experimentally, with separate feedback

regulation of the input flow rate for the two different chemical species. They found that a bursting phenomena can be caused by feedback control, where oscillations and uniform solutions alternate in time. [10] obtained experimental results for a nickel-sulfuric acid electrochemical system. This system exhibits limit cycle solutions which were successfully controlled by both simple time delay feedback and a weighted method which used feedback from many previous solution times. A copper-phosphoric acid system was also considered with the aim of controlling chaotic behaviour.

Commonly the CSTR is considered as an open system with the supply of reactant at a fixed rate. Alternatively a closed system can be considered where the supply of reactant results from the decay of a precursor chemical which is present at a large fixed concentration in the CSTR. This is the pooled chemical approximation; [15] examined a simple pooled chemical reaction model for cubic autocatalysis in a closed CSTR. They found the value of rate constant associated with precursor decay when the stable limit cycle was generated and Hopf bifurcations disappeared. [17] considered transient chaos in a closed chemical system. The authors studied an extension of the Brusselator model, governed by a set of four odes, which involved the transformation of a relatively stable precursor to a final product through three intermediate species. They considered that sensitivity of solutions to initial conditions, which is a major characteristic of chaos.

In a reaction diffusion cell the system is an open one and the supply of reactant occurs via diffusion from a boundary reservoir, see, for example, [12]. The effect of a precursor chemical can be considered in a reaction diffusion cell by including the precursor in the boundary reservoir. The reactant is then supplied directly by diffusion into the cell and indirectly by diffusion of the precursor and its subsequent decay. [2] considered this scenario for a cubic autocatalytic reaction and found that the concentration of the precursor is not constant in the cell. The authors studied the effect of precursor rate constant on the formation of bifurcation diagrams and Hopf regions. They found that increasing the precursor rate constant led to a dramatic shift in the parameter region in which Hopf bifurcations occur.

In this paper, the full reversible Selkov model (1) is modelled in a 1-D reaction-diffusion cell. The reactions associated with the both the precursor and the final product are included in the model. In §2 the governing equations are presented and the Galerkin method is used to obtain the odes which represent the semi-analytical model. In §3 the steady-state concentration profiles and bifurcation patterns are presented and described in detail. In §4 the hysteresis bifurcation points is calculated by using singularity theory. The regions of parameter space are found in which the two main bifurcation patterns occur. In §5 a local stability analysis of the semi-analytical model is performed. The Hopf points are found; hence the parameter region in which Hopf bifurcations occur is identified. The effect of two key parameters, which do not occur in the model of [1], are explored in detail. These parameters are the rate constants associated with the decay rate of the precursor and the

(reverse step) decay of the final product. Comparisons are made throughout the paper between the semi-analytical results and numerical solutions of the governing pdes.

2 The semi-analytical model

2.1 The governing equations

The reversible Selkov model (1), is considered in a 1-D reaction-diffusion cell. The governing pdes are

$$\begin{aligned} s_t &= D_1 s_{xx} - \kappa s - s p^2 + K_2 p^3 + \mu_1 a, \\ p_t &= D_2 p_{xx} - p + s p^2 - K_2 p^3 + \mu_2 b, \qquad (2) \\ a_t &= a_{xx} - \mu_1 a + \kappa s, \quad b_t = b_{xx} - \mu_2 b + p, \\ s_x &= p_x = a_x = b_x = 0, \text{ at } x = 0 \qquad (3) \\ s &= s_0, p = p_0, a = a_0, b = b_0 \text{ at } x = 1 \text{ and } t = 0. \end{aligned}$$

The system (2) is in non-dimensional form with the scaled concentrations of the four chemical species, the reactant, s, autocatalyst, p, the precursor reactant, a and the final product, b. This system is an open system; the reactor has a permeable boundary at $x = 1$, joined to a reservoir which contains s, p, a and b at specified concentrations, s_0, p_0, a_0 and b_0, respectively. The boundary condition at $x = 0$ is a zero-flux condition. (2) and (3) represents a system characterized by ten non-dimensional parameters. The rate constants, associated with the forward and backwards steps, for the first of (1) are μ_1 and κ, respectively. For the second of (1) the rate constants are 1 and K_2 while for the third of (1) the rate constants are 1 and μ_2. The parameters D_1 and D_2 denote the diffusion coefficients of the two species s and p. In [1] it was assumed that the decay of the precursor chemical $A \to S$ and the backwards reaction of the final product $P \leftarrow B$ were small and could be neglected. This assumption means that $\mu_1 = \mu_2 = 0$ and the system (3) reduces to the two coupled pdes considered in [1]. Here, though we assume that these reaction rates are finite and can not be ignored. This means that the a and final product b are governed by their own pdes and a much larger set of four coupled pdes governs the dynamics of the reversible Selkov model.

The effect of feedback on the reaction-diffusion cell (2) and (3) is also of significant interest, so we consider the the following feedback algorithm

$$\begin{aligned} s_x = p_x = a_x = b_x, \text{ at } x = 0, \\ s = s_0 + H(s(0,t) - s_s), \quad p = p_0 + H(p(0,t) - p_s), \qquad (4) \\ a = a_0 + H(a(0,t) - a_s), \quad b = b_0 + H(b(0,t) - b_s), \text{ at } x = 1, \end{aligned}$$

where s_s, p_s, a_s and b_s are the steady-state concentrations at $x = 0$. The reservoir concentrations are changed, in response to the concentrations in the

cell at the impermeable boundary at $x = 0$. The feedback mechanism causes the reservoir concentrations to vary in response to the difference between the concentration at the center of the cell and the steady-state value, while H is the strength of the feedback response. Here, the effect of this feedback control algorithm on the stability of reaction-diffusion cell is investigated. (4) does not alter the steady-state solution of (3). Note that this feedback algorithm is only physically realistic if the concentrations of the various chemical species remain positive. This will occur if the solution is close to the steady-state, $|s(0,t) - s_s| \ll 1$ (and equivalent expressions for the other species) or the strength of the feedback is small, $|H| \ll 1$. Numerical solutions of (2) are found using an explicit finite-difference scheme with accuracy of $O(\triangle t, \triangle x^2)$.

2.2 The Galerkin method

The Galerkin method is used and assumes a spatial structure for the concentration profiles. This allows the governing pdes (2) and boundary conditions (4) to be approximated by a set of lower-order odes. The expansion

$$\begin{aligned}
s(x,t) &= s_0 + H(s_1(t) + s_2(t) - s_{1s} - s_{2s}) + s_2(t)\cos(\frac{3}{2}\pi x) \\
&+ (s_1(t) - H(s_1(t) + s_2(t) - s_{1s} - s_{2s}))\cos(\frac{1}{2}\pi x), \\
p(x,t) &= p_0 + H(p_1(t) + p_2(t) - p_{1s} - p_{2s}) + p_2(t)\cos(\frac{3}{2}\pi x) \\
&+ (p_1(t) - H(p_1(t) + p_2(t) - p_{1s} - p_{2s}))\cos(\frac{1}{2}\pi x), \\
a(x,t) &= a_0 + H(a_1(t) + a_2(t) - a_{1s} - a_{2s}) + a_2(t)\cos(\frac{3}{2}\pi x) \\
&+ (a_1(t) - H(a_1(t) + a_2(t) - a_{1s} - a_{2s}))\cos(\frac{1}{2}\pi x) \\
b(x,t) &= b_0 + H(b_1(t) + b_2(t) - b_{1s} - b_{2s}) + b_2(t)\cos(\frac{3}{2}\pi x) \\
&+ (b_1(t) - H(b_1(t) + b_2(t) - b_{1s} - b_{2s}))\cos(\frac{1}{2}\pi x),
\end{aligned} \tag{5}$$

represents the two-term method which is used here. Expansion (5) satisfies the boundary conditions in (4), but not the governing pdes. The form of basis functions (5) are chosen so the concentrations at the impermeable boundary $x = 0$ are $s = s_0 + s_1 + s_2$, with similar expressions for the other concentrations. The free parameters in (5) are found by evaluating averaged versions of the governing equations, weighted by the basis functions. This technique gives the odes

$$\begin{aligned}
\frac{ds_1}{dt} &= \frac{4K_2p_0^3}{\pi} - \frac{4\kappa s_0}{\pi} - \frac{4s_0p_0^2}{\pi} - s_1p_0^2 - \frac{3s_1p_1^2}{4} + \frac{3K_2p_1^3}{4} - \kappa s_1 - \frac{s_2p_1^2}{4} \\
&- \frac{s_1p_1p_2}{2} + \frac{3K_2p_1p_2^2}{2} + \frac{3K_2p_1^2p_2}{4} - 2s_0p_0p_1 - \frac{D_1s_1\pi^2}{4} + 3K_2p_0^2p_1 - \frac{72s_0p_2^2}{35\pi}
\end{aligned}$$

$$
\begin{aligned}
&-\frac{8s_0p_1^2}{3\pi} - s_2p_1p_2 + \frac{16K_2p_0p_1p_2}{5\pi} - \frac{16s_0p_1p_2}{15\pi} - \frac{16s_1p_0p_2}{15\pi} - \frac{16s_2p_0p_1}{15\pi} \\
&+\frac{8K_2p_0p_1^2}{\pi} - \frac{16s_1p_0p_1}{3\pi} - \frac{144s_2p_0p_2}{35\pi} + \frac{216K_2p_0p_2^2}{35\pi} + \frac{4\mu_1a_0}{\pi} + \mu_1a_1 - \frac{s_1p_2^2}{2}. \\
&\frac{dp_1}{dt} = \frac{4s_0p_0^2}{\pi} - p_1 - \frac{4p_0}{\pi} - \frac{4K_2p_0^3}{\pi} + s_1p_0^2 + \frac{3s_1p_1^2}{4} - \frac{3K_2p_1^3}{4} + \frac{s_2p_1^2}{4} + \frac{s_1p_2^2}{2} \\
&+\frac{s_1p_1p_2}{2} - \frac{3K_2p_1p_2^2}{2} - \frac{3K_2p_1^2p_2}{4} + 2s_0p_0p_1 - 3K_2p_0^2p_1 + \frac{72s_0p_2^2}{35\pi} + \frac{8s_0p_1^2}{3\pi} \\
&-\frac{16K_2p_0p_1p_2}{5\pi} + \frac{16s_0p_1p_2}{15\pi} + \frac{16s_1p_0p_2}{15\pi} + \frac{16s_2p_0p_1}{15\pi} - \frac{8K_2p_0p_1^2}{\pi} + \frac{144s_2p_0p_2}{35\pi} \\
&-\frac{216K_2p_0p_2^2}{35\pi} + \frac{4\mu_2b_0}{\pi} + \mu_2b_1 - \frac{D_2p_1\pi^2}{4} + s_2p_1p_2, \\
&\frac{ds_2}{dt} = \frac{4\kappa s_0}{3\pi} - \kappa s_2 - \frac{9D_1s_2\pi^2}{4} + \frac{4s_0p_0^2}{3\pi} - \frac{4K_2p_0^3}{3\pi} - \frac{3s_2p_2^2}{4} - s_2p_0^2 + \frac{3K_2p_2^3}{4} \\
&-\frac{K_2p_1^3}{4} - \frac{s_2p_1^2}{2} + 3\kappa p_0^2p_2 - 2s_0p_0p_2 - s_1p_1p_2 + \frac{3K_2p_1^2p_2}{2} + \frac{8s_0p_2^2}{9\pi} - \frac{8s_0p_1^2}{15\pi} \\
&+\frac{432K_2p_0p_1p_2}{35\pi} - \frac{144s_0p_1p_2}{35\pi} - \frac{144s_1p_0p_2}{35\pi} - \frac{144s_2p_0p_2}{35\pi} + \frac{8K_2p_0p_1^2}{5\pi} - \frac{16s_1p_0p_1}{15\pi} \\
&+\frac{16s_2p_0p_2}{9\pi} - \frac{8K_2p_0p_2^2}{3\pi} - \frac{4\mu_1a_0}{3\pi} + \mu_1a_2 - \frac{s_1p_1^2}{4}, \qquad (6) \\
&\frac{dp_2}{dt} = \frac{4p_0}{3\pi} - p_2 - \frac{9D_2p_2\pi^2}{4} - \frac{4s_0p_0^2}{3\pi} + \frac{4K_2p_0^3}{3\pi} + \frac{3s_2p_2^2}{4} + s_2p_0^2 - \frac{3K_2p_2^3}{4} \\
&-\frac{K_2p_1^3}{4} + \frac{s_2p_1^2}{2} - 3\kappa p_0^2p_2 + 2s_0p_0p_2 + s_1p_1p_2 - \frac{3K_2p_1^2p_2}{2} - \frac{8s_0p_2^2}{9\pi} + \frac{8s_0p_1^2}{15\pi} \\
&-\frac{432K_2p_0p_1p_2}{35\pi} + \frac{144s_0p_1p_2}{35\pi} + \frac{144s_1p_0p_2}{35\pi} + \frac{144s_2p_0p_2}{35\pi} - \frac{8K_2p_0p_1^2}{5\pi} + \frac{16s_1p_0p_1}{15\pi} \\
&-\frac{16s_2p_0p_2}{9\pi} + \frac{8K_2p_0p_2^2}{3\pi} - \frac{4\mu_2b_0}{3\pi} + \mu_2b_2 + \frac{s_1p_1^2}{4}, \\
&\frac{da_1}{dt} = \frac{4\kappa s_0}{\pi} - \frac{4\mu_1a_0}{\pi} - \frac{a_1\pi^2}{4} + \kappa s_1 - \mu_1a_1, \\
&\frac{db_1}{dt} = \frac{4p_0}{\pi} - \frac{4\mu_2b_0}{\pi} - \frac{b_1\pi^2}{4} + p_1 - \mu_2b_1, \\
&\frac{da_2}{dt} = \frac{4\kappa s_0}{3\pi} - \frac{4\mu_1a_0}{3\pi} - \frac{9a_2\pi^2}{4} + \kappa s_2 - \mu_1a_2, \\
&\frac{db_2}{dt} = \frac{4\mu_2b_0}{3\pi} - \frac{4p_0}{3\pi} - \frac{9b_2\pi^2}{4} + p_2 - \mu_2b_2.
\end{aligned}
$$

This set of odes (6) gives the case of no feedback ($H = 0$) as the feedback terms are too long to be presented here. It is found that a two-term method gives sufficient accuracy without excessive expression swell. The one-term solution (when $s_2 = p_2 = a_2 = b_2 = 0$) is also calculated, for accuracy comparison purposes.

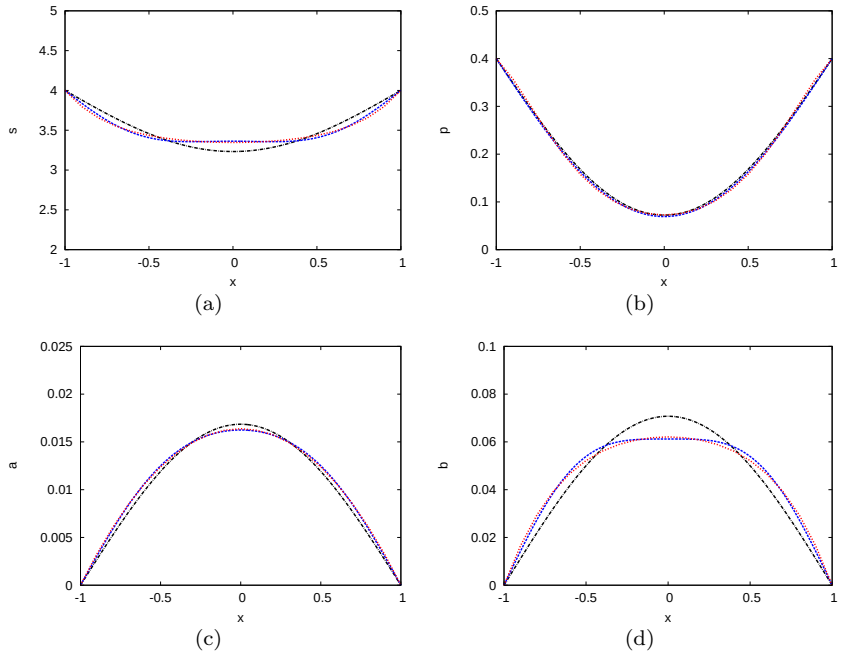

Figure 1: Steady-state concentration profiles, s, p, a and b versus x. The parameters are $s_0 = 4$, $\kappa = 0.01$, $D_1 = D_2 = 0.08$, $a_0 = b_0 = 0$, $K_2 = 1$, $p_0 = 0.4$ and $\mu_1 = \mu_2 = 0.1$. The one-term (black solid line), two-term (blue dashed line) semi-analytical solutions and the numerical solution of (2) (red dashed line) are shown.

3 Steady-state solutions

At the steady-state all the time derivative terms in (6) are zero so a set of eight transcendental equations are obtained. These equations are manipulated to find explicit expressions for a_1, a_2, b_1 and b_2, which are substituted back into the remaining equations in (6). We then obtain four transcendental equations, $f_i = 0 \quad i = 1, \ldots, 4$, for the other unknowns s_1, s_2, p_1 and p_2, which are solved numerically using Maple.

Figures 1(a) to 1(d) show steady-state concentration profiles for s, p, a and b versus x. The parameters are $s_0 = 4$, $D_1 = D_2 = 0.08$, $p_0 = 0.4$, $\mu_1 = \mu_2 = 0.1$, $a_0 = b_0 = 0$. The one and two-term semi-analytical solutions and the numerical solution of (2) are shown. For this choice of parameters the reactant s and autocatalyst p are consumed in the cell, as their profiles show a central trough. The profile of both the precursor a and final product b show a central peak so are created in the cell. For the reaction $A \rightleftharpoons S$, the backward step dominates the forwards one, due to the high concentration of s, relative

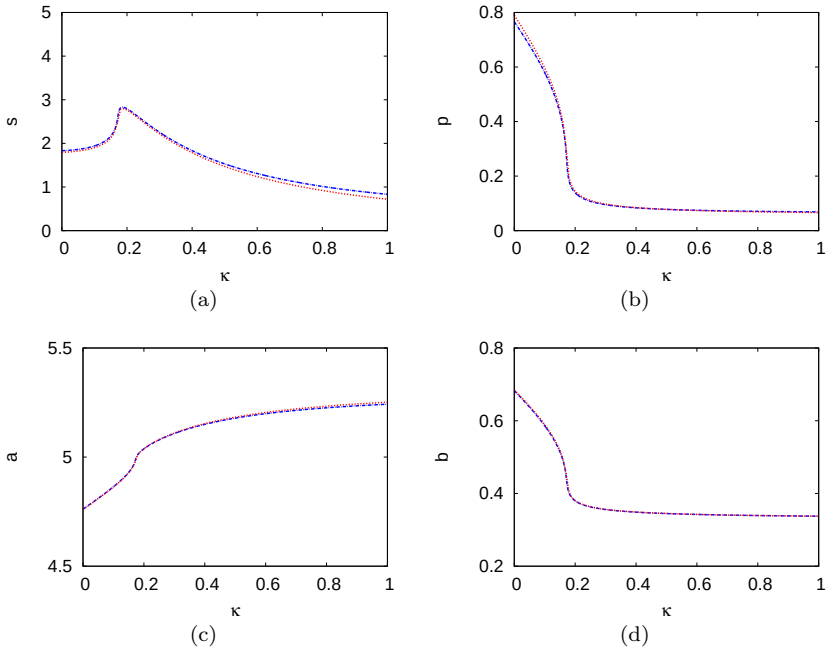

Figure 2: Steady-state bifurcation diagrams, s, p, a and b versus κ. The concentrations are shown at $x = 0$. The parameters are $s_0 = 4$, $D_1 = D_2 = 0.08$, $p_0 = 0.4$, $\mu_1 = \mu_2 = 0.1$, $a_0 = 5$ and $b_0 = 0.3$. The two-term (blue dash-dotted line) semi-analytical solutions and the numerical solution of (2) (red dotted line) are shown.

to a, while for $P \rightleftharpoons B$ the forward step dominates the backwards one, due to the high concentration of p relative to b. The two-term semi-analytical solution is very accurate; when compared with the numerical solution of the governing pdes. Errors at the centre of the cell are less than 4%, for all the concentrations. The one term semi-analytical solutions are less accurate with errors of up to 15% in the concentration profiles. The two-term solutions are more accurate as they can model the flat concentration profiles better.

Figures 2(a) to 2(d) show bifurcation diagrams for s, p, a and b versus κ. The parameters are $s_0 = 4$, $D_1 = D_2 = 0.08$, $p_0 = 0.4$, $\mu_1 = \mu_2 = 0.1$, $a_0 = 5$ and $b_0 = 0.3$. The two-term semi-analytical and numerical solutions of (2) are shown. The bifurcation diagrams display the steady-state concentrations at the centre of the reactor, at $x = 0$, versus κ the bifurcation parameter. This figure shows an unique pattern, with the steady state concentrations for s, p and b decreasing for large κ, while the steady-state concentration a increases for large κ. The creation of precursor increases for large κ as the importance as the backward step of the reaction $A \rightleftharpoons S$, increases. At $\kappa = 0.4$ the numer-

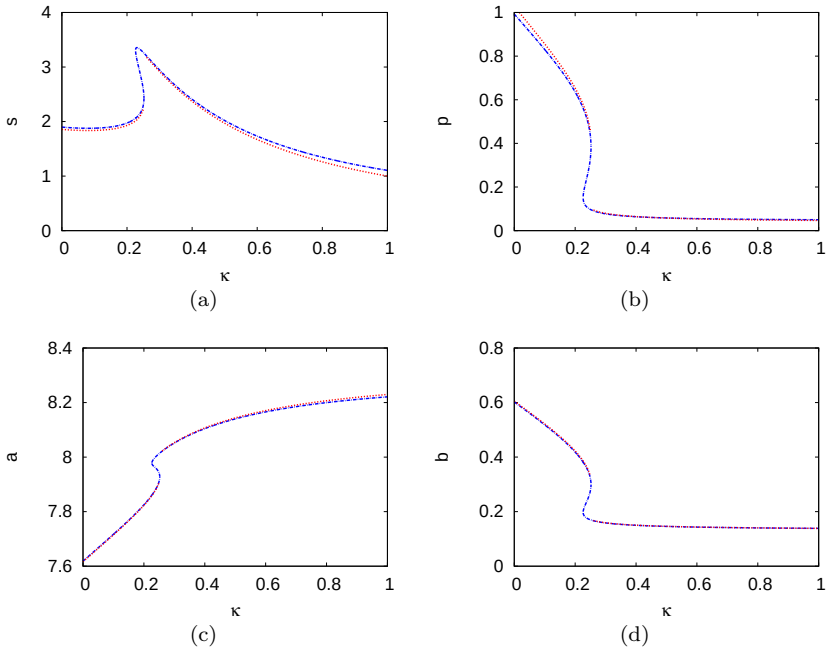

Figure 3: Steady-state bifurcation diagrams, s, p, a and b versus κ. The concentrations are shown at $x = 0$. The parameters are $s_0 = 4$, $D_1 = D_2 = 0.08$, $p_0 = 0.4$, $\mu_1 = \mu_2 = 0.1$, $a_0 = 8$ and $b_0 = 0.1$. The two-term (blue dash-dotted line) semi-analytical solutions and the numerical solution of (2) (red dotted line) are shown.

ical solutions are $(s, p, a, b) = (1.785, 0.085, 5.153, 0.349)$ while the two-term semi-analytical solutions are $(s, p, a, b) = (1.834, 0.084, 5.150, 0.349)$. The two-term solution is very close to the numerical solution of the pdes. The errors between the numerical and two-term semi-analytical solutions are less than 3%.

Figures 3(a) to 3(d) show bifurcation diagrams for s, p, a and b versus κ. The parameters are $s_0 = 4$, $D_1 = D_2 = 0.08$, $K_2 = 1$, $p_0 = 0.4$, $\mu_1 = \mu_2 = 0.1$, $a_0 = 8$ and $b_0 = 0.1$. The two-term semi-analytical and numerical solutions of (2) are shown. This is a breaking wave pattern (only two different patterns are possible for this system) so a bifurcation point exists where the solution jumps from a high autocatalyst conversion state to a low conversion state at $\kappa = 0.226$. At the bifurcation point the concentration of reactant and precursor both increase while the concentration of the final product drops. The two-term semi-analytical results are very accurate with a variation of less than 7% with numerical solutions for all the parameter values shown on the figures.

4 Singularity theory

Singularity theory allows a full description of all qualitatively different steady-state behaviors, for a system of odes. This is achieved by calculating the degenerate singular points. [8] provides an overview of singularity theory while [3] considers applications of singularity theory to chemical reactions. The authors presented the hysteresis and isola bifurcation curves conditions and applied singularity theory to some models involving first-order, non-isothermal reactions in a CSTR.

In this paper, we will apply singularity theory to the semi-analytical model of §2. This will provide a semi-analytical description of the parameter regions in which the two main types of bifurcation pattern, unique and breaking wave, occurs. The steady-state equations, two-term model can be written in the form

$$f_i(p_1, p_2, s_1, s_2, \kappa, s_0, p_0, a_0, b_0) = 0, \quad i = 1, \dots 4, \tag{7}$$

where κ is the choice of bifurcation parameter. The hysteresis bifurcation is found, in the κ versus p_1 plane, by applying the following conditions

$$\frac{d\kappa}{dp_1} = \frac{d^2\kappa}{dp_1^2} = 0. \tag{8}$$

As the equations (7) do not provide an explicit relationship for κ the conditions (8) must be applied implicitly. The total derivative of (7) with respect to p_1 is given by

$$\frac{df_i}{dp_1}(p_1, p_2, s_1, s_2) = f_{ip_1} + f_{ip_2}\frac{dp_2}{dp_1} + f_{is_1}\frac{ds_1}{dp_1} + f_{is_2}\frac{ds_2}{dp_1} = 0, \quad i = 1, \dots 4, \tag{9}$$

where the first of (8) has been applied and the other parameters are constant for a given bifurcation diagram. In (9) the f_i are functions of p_1, p_2, s_1 and s_2 which means the f_i depend on p_1 both explicitly and implicitly via the other variables. The second total derivative of (7) is given by

$$\frac{d^2 f_i}{dp_1^2}(p_1, p_2, s_1, s_2) = 0, \quad i = 1, \dots 4. \tag{10}$$

For the two-term model, the hysteresis bifurcation points are given by solving (7), (9) and (10) using Maple.

Figure 4 shows the division of the s_0-p_0 plane into regions corresponding to the two different bifurcation diagrams. Shown is the hysteresis curve with $\mu_1 = \mu_2 = 0$, 0.1, 0.3 and 0.5. The other parameters are $D_1 = D_2 = 0.08$, $a_0 = 1$ and $b_0 = 0$. Shown is the two-term hysteresis curve (7), (9) and (10). On the left side of the hysteresis curve the unique bifurcation pattern occurs while on the right side of the curve the breaking-wave pattern occurs. The figure shows that increasing the rate constants μ_1 and μ_2 leads to the hysteresis curve moving to the left with the breaking-wave pattern possible for smaller values of s_0.

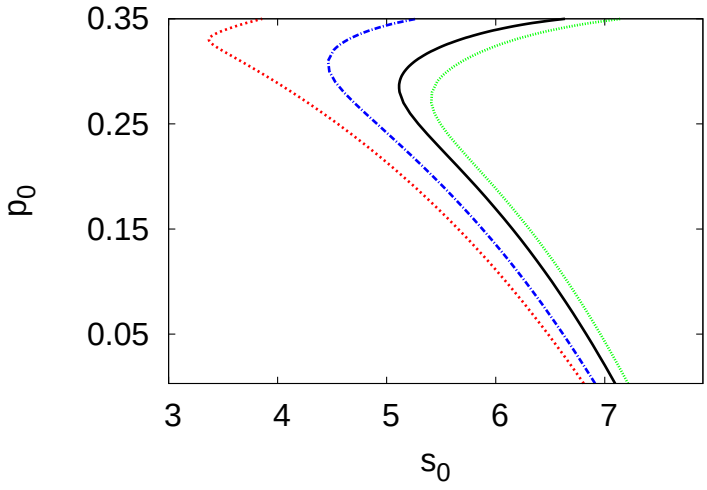

Figure 4: Division of the s_0-p_0 plane into regions corresponding to the different bifurcation diagrams. Shown is the two-term semi-analytical curve with $\mu_1 = \mu_2 = 0$ (green small dotted line), 0.1 (black solid line), 0.3 (blue dash-dotted line) and 0.5 (red dotted line). The parameters are $D_1 = D_2 = 0.08$, $a_0 = 1$ and $b_0 = 0$.

Figure 5 shows the division of the a_0-b_0 plane into regions corresponding to the different bifurcation diagrams. Shown is the hysteresis curve with $\mu_1 = \mu_2 = 0.1$, 0.3 and 0.5. The other parameters are $D_1 = D_2 = 0.08$, $s_0 = 4$ and $p_0 = 0.4$. Shown is the two-term hysteresis curve (7), (9) and (10). Above the hysteresis curves the unique bifurcation pattern occurs while under the curves the breaking-wave pattern occurs. As the rate constants for the precursor and final product increase the hysteresis curve moves to the left allowing the breaking-wave pattern to occur for small values of a_0. The example of figure 2, with parameters $a_0 = 5$ and $b_0 = 0.3$ and $\mu_1 = \mu_2 = 0.1$, lies above the relevant curve in figure 5 hence is an unique pattern while the example of figure 3 with parameters $a_0 = 8$ and $b_0 = 0.1$ and $\mu_1 = \mu_2 = 0.1$, lies below the curve hence is a breaking wave pattern.

5 Local stability and oscillatory solutions

The theory of Hopf bifurcations is explained in standard texts on bifurcation theory and dynamical systems such as [8, 9]. Here the stability of the semi-analytical model is analyzed and used to explore the effects of the reaction rates for the precursor and final product in altering the stability of the system

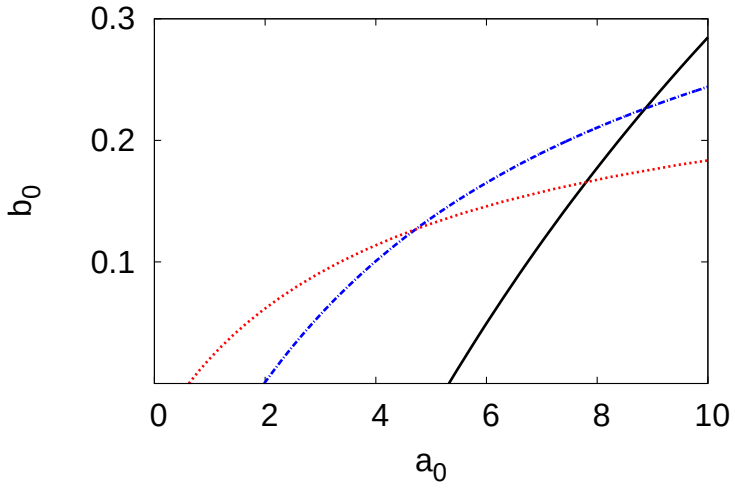

Figure 5: Division of the a_0-b_0 plane into regions corresponding to the different bifurcation diagrams. Shown is the two-term semi-analytical curve with $\mu_1 = \mu_2 = 0.1$ (black solid line), 0.3 (blue dash-dotted line) and 0.5 (red dotted line). The parameters are $D_1 = D_2 = 0.08$, $s_0 = 4$ and $p_0 = 0.4$.

(2). The Hopf degeneracy points are calculated to find a semi-analytical map in which Hopf bifurcations and limit cycles occur and this prediction is compared with numerical results. In this paper, Hopf points are obtained by expanding in a Taylor series about the steady-state solution,

$$\begin{aligned} s_i(t) &= s_{is} + \epsilon g_i e^{-\lambda t}, \quad & p_i(t) &= p_{is} + \epsilon \delta_i e^{-\lambda t}, \\ a_i(t) &= a_{is} + \epsilon h_i e^{-\lambda t}, \quad & b_i(t) &= b_{is} + \epsilon \beta_i e^{-\lambda t}, \quad i = 1, 2. \end{aligned} \tag{11}$$

We substitute (11) into the odes (6), and linearize around the steady state. The eigenvalues of the Jacobian matrix characterizes nature of the perturbation to the system and we obtain a characteristic equation for λ. We set $\lambda = i\omega$ in the characteristic equation and separate the real q_1 and imaginary q_2 parts. The Hopf bifurcation points occur at points where λ is purely imaginary, see [16]. Here we look for Hopf bifurcation points together with the condition $\kappa = 0$ which represents physically realistic Hopf bifurcations. The conditions are

$$f_i = 0, \quad i = 1, \ldots 4, \quad q_1 = q_2 = \kappa = 0. \tag{12}$$

Figure 6 shows the region of the s_0-p_0 plane in which Hopf bifurcation can occur. Shown are the two-term solutions (12) plus numerical solutions. The parameters are $D_1 = D_2 = 0.08$, $\mu_1 = \mu_2 = 0.1$, $a_0 = 1$ and $b_0 = 0$. The looped curve encloses the region in which physically realistic Hopf bifurcation

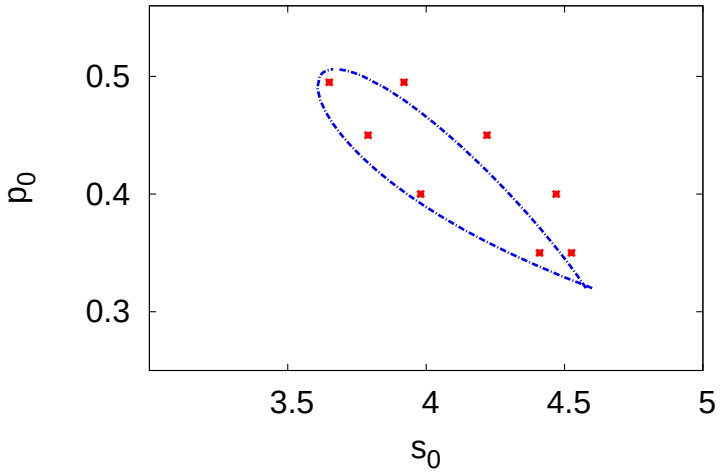

Figure 6: The region of the s_0-p_0 plane in which physically realistic Hopf bifurcation can occur. The two term (blue dashed line) region and numerical solutions (red squares) are shown. The parameters are $D_1 = D_2 = 0.08$, $\mu_1 = \mu_2 = 0.1$, $a_0 = 1$ and $b_0 = 0$.

points occur, with $\kappa > 0$, while outside the region all the physically realistic solutions are stable. Hence Hopf bifurcations only occur in a small region of parameter space, $s_0 \in (3.61, 4.60)$ and $p_0 \in (0.31, 0.51)$. The comparisons between the semi-analytical estimates and the numerical solutions, of the pde model, are excellent. For example, at $p_0 = 0.35$, the maximum numerical value at which Hopf bifurcations can occur is $s_0 = 4.53$ while the two-term semi-analytical maximum value is $s_0 = 4.49$, which represents a difference of less than 1%.

Figure 7 shows the region of the a_0-b_0 plane in which Hopf bifurcation can occur. The two-term semi-analytical solutions (12) and numerical solutions are shown. The other parameters are $D_1 = D_2 = 0.08$, $\mu_1 = \mu_2 = 0.1$, $s_0 = 4$ and $p_0 = 0.4$. Here the loop crosses the a_0-axis so only part of the loop is in positive parameter space. Again, inside the looped curve physically realistic limit cycles can occur while outside the loop the physically realistic solutions are stable. The comparison between the two-term semi-analytical and numerical solutions, of the pde model, is very good. For example, at $b_0 = 0.15$ the minimum and maximum numerical values at which limit cycles occur is $a_0 = 0.38$ and $a_0 = 1.12$ while the two term semi-analytical predictions are $a_0 = 0.30$ and $a_0 = 0.96$; the differences in these estimates is less than 20%.

Figure 8 shows the regions of the $s_0 - p_0$ plane in which Hopf bifurcations can occur, for $\mu_1 = \mu_2 = 0$, 0.1, 0.15 and 0.17. The other parameters are

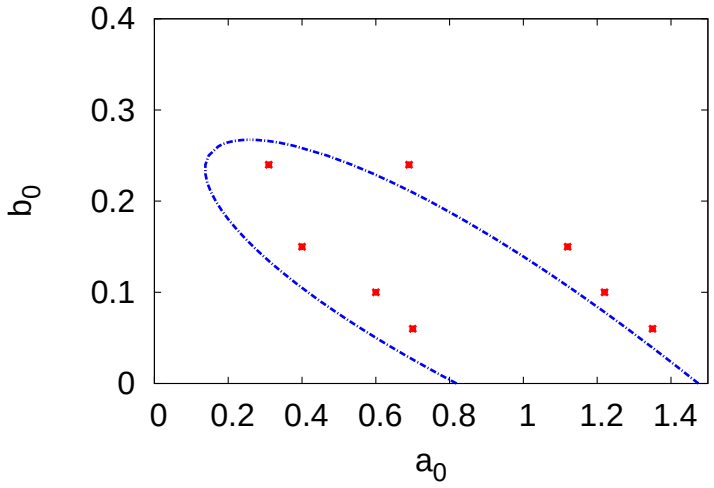

Figure 7: The region of the a_0-b_0 plane in which physically realistic Hopf bifurcation can occur. The two term (blue dashed lines) region and numerical solutions (red squares). The parameters are $D_1 = D_2 = 0.08$, $\mu_1 = \mu_2 = 0.1$,$s_0 = 4$ and $p_0 = 0.4$.

$D_1 = D_2 = 0.08$, $a_0 = 1$ and $b_0 = 0$. As the rate constants, μ_1 and μ_2, are increased the looped curves move to the left and the area of the curves decreases. The looped curve of Hopf region disappears for $\mu_1 = \mu_2 > 0.4$, so for large reaction rates limit cycles do not occur. Figure 9 shows the regions of the $a_0 - b_0$ plane in which Hopf bifurcations can occur, for $\mu_1 = \mu_2 = 0.1$, 0.17 and 0.2. The other parameters are $D_1 = D_2 = 0.08$, $s_0 = 4$ and $p_0 = 0.4$. Similar to figure 8, it can be clearly see that increasing reaction rates μ_1 and μ_2 causes the looped curve to move leftwards and reduce in area. All the looped regions intersect the a_0 axis so physically realistic limit cycles only occur for parameter values in the positive quarter plane.

Figure 10 shows Hopf bifurcation regions in the $s_0 - p_0$ plane, for different positive values of feedback response $H = 0$, 0.1 and 0.2. The other parameters are $D_1 = D_2 = 0.08$, $\mu_1 = \mu_2 = 0.1$, $a_0 = 1$ and $b_0 = 0.1$. An increase occurs in the area of the looped region as the feedback strength increases. Hence positive values of the feedback strength H destabilizes the system. For example the point (s_0, p_0)=(3.60, 0.54) is stable when $H = 0$ however, it is unstable for both $H = 0.1$ and 0.2.

Figure 11 shows Hopf bifurcation regions in the $a_0 - b_0$ plane, for different positive values of feedback strength $H = 0$, 0.03 and 0.05. The other parameter values are $D_1 = D_2 = 0.08$, $\mu_1 = \mu_2 = 0.1$, $s_0 = 4$ and $p_0 = 0.4$. It can be seen that the region of instability is increased as the feedback strength

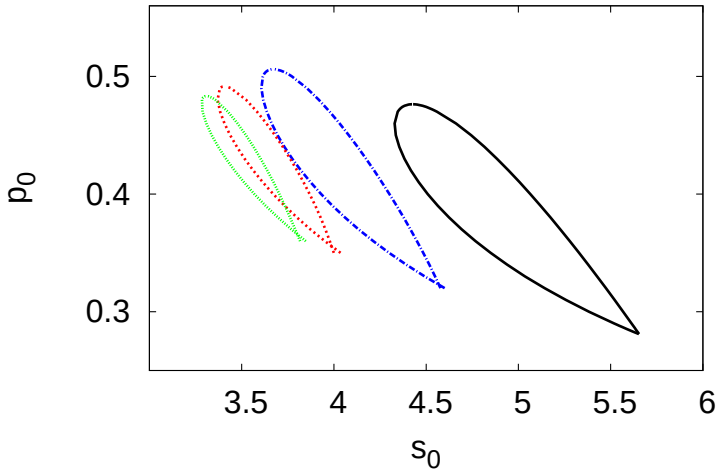

Figure 8: The regions Hopf bifurcation occur in s_0-p_0 plane. The parameters $\mu_1 = \mu_2 = 0$ (black solid lines), 0.1 (blue dash-dotted lines), 0.15 (red dotted lines) and $\mu_1 = \mu_2 = 0.17$ (green short dotted lines). The other parameters are $D_1 = D_2 = 0.08$, $a_0 = 1$ and $b_0 = 0$.

H increases, a similar effect to that which occurs in the $s_0 - p_0$ plane. For example, the point (a_0, b_0)=$(0.20, 0.28)$ is stable for $H = 0$, but it is unstable when both $H = 0.03$ and 0.05. As H increases the loop crosses the b_0-axis (for $H = 0.04$) and into a region of unphysical solutions, where a_0 is negative.

Figure 12 shows Hopf bifurcation regions in the s_0-p_0 plane, for negative values of feedback response $H = 0$, -0.05 and -0.1. The other parameters are $D_1 = D_2 = 0.08$, $\mu_1 = \mu_2 = 0.1$, $a_0 = 1$ and $b_0 = 0.1$. It can be seen that the looped region is reduced in area as the magnitude of the negative feedback strength H increases, stabilizing the system. For example the point (s_0, p_0)=$(3.70, 0.45)$ is unstable when $H = 0$ however, it is stable for both $H = -0.05$ and -0.1. The looped region disappears at $H = -0.21$, so for H less than this value no limit cycles occur.

Figure 13 shows Hopf regions in the $a_0 - b_0$ plane, for negative values of the feedback strength $H = 0$, -0.1 and -0.15. The other parameter values are $D_1 = D_2 = 0.08$, $\mu_1 = \mu_2 = 0.1$, $s_0 = 4$ and $p_0 = 0.4$. The region of instability is decreased as the magnitude of the negative feedback strength H increases. For example, the point (a_0, b_0)=$(0.40, 0.15)$ is unstable for $H = 0$ but, it is stable when both $H = -0.1$ and 0.15. while the point (a_0, b_0)=$(0.61, 0.10)$ is unstable for both $H = 0$ and -0.1 while stable when $H = -0.15$.

Figure 14(a) and (b) shows limit cycle solutions in the s versus p and

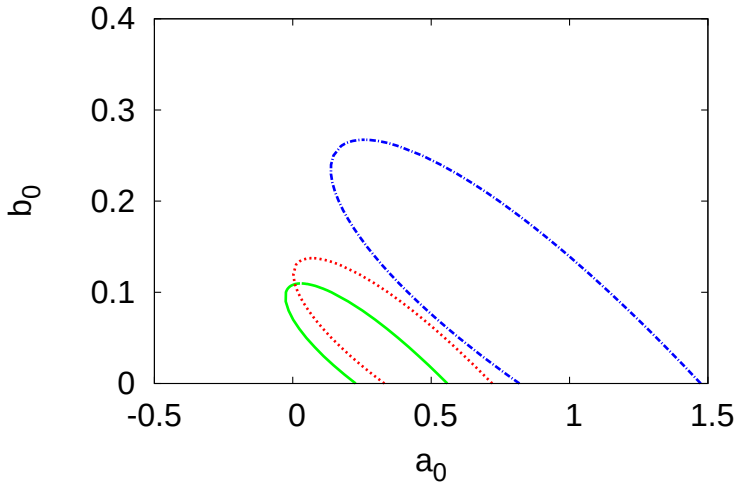

Figure 9: The regions Hopf bifurcation occur in a_0-b_0 plane. The parameters $\mu_1 = \mu_2 = 0.1$ (blue dash-dotted lines), 0.17 (red dotted lines) and 0.2 (green solid lines). The other parameters are $D_1 = D_2 = 0.08$, $s_0 = 4$ and $p_0 = 0.4$.

a versus b phase planes. Figures 14(c), 14(d), 14(e) and 14(f) show the evolution of s, p, a and b versus t, respectively, at $x = 0$. The parameters are $s_0 = 4$, $p_0 = 0.4$, $D_1 = D_2 = 0.08$, $\mu_1 = \mu_2 = 0.1$, $a_0 = 0.8$, $b_0 = 0.15$, $H = 0$ and $\kappa = 0.001$. Shown are the two-term semi-analytical solution and the numerical solution. These parameters fall inside the looped region of figure 11 so a limit cycle occurs. The two-term semi-analytical period of the limit cycle is 25.7 and the amplitudes are 1.526, 0.406, 0.001 and 0.182 for the reactant, autocatalyst, precursor, and final product concentrations respectively. The numerical period is 26.6 while, the amplitudes of concentrations in the limit cycles are 1.558, 0.421, 0.001 and 0.186. The errors in the two-term semi-analytical values, compared to numerical solutions of (2) are less than 4%. Also the time evolution curves show that the locations of the first few peaks and troughs of the semi-analytical solutions are close to the numerical values.

Figures 15(a), (b), (c) and (d) show the evolution of s, p, a and b versus t, at $x = 0$. The parameters are $s_0 = 4$, $p_0 = 0.4$, $D_1 = D_2 = 0.08$, $\mu_1 = \mu_2 = 0.1$, $a_0 = 0.4$, $b_0 = 0.3$, $H = 0$ and $\kappa = 0.02$. Shown are two-term semi-analytical solution and the numerical solution. In this case the parameter values lie outside the looped region in figure 11 for $H = 0$, so a steady-state solutions occurs. So as the time becomes large, the two-term semi-analytical solution evolves to the steady-state $(s, p, a, b) \simeq (2.74, 0.20, 0.41, 0.41)$ while the numerical steady-state solution is $(2.71, 0.21, 0.41, 0.41)$. The errors between two-term semi-analytical solutions and numerical solutions less than

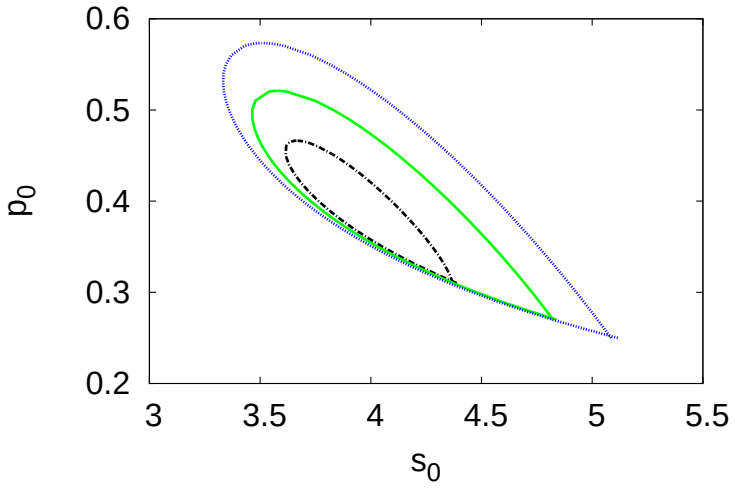

Figure 10: Hopf bifurcation curves in the $s_0 - p_0$ plane. Shown is the two-term semi-analytical solutions with feedback strength $H = 0$ (black dashed line), $H = 0.1$ (green solid line) and $H = 0.2$ (blue small dotted line). The other parameters are $D_1 = D_2 = 0.08$, $\mu_1 = \mu_2 = 0.1$, $a_0 = 1$ and $b_0 = 0.1$.

5%. It can be seen that the comparison between the two-term semi-analytical and numerical solutions of the governing pdes, of the steady-state values and of the relaxation oscillations, is excellent.

6 Conclusion

Semi-analytical solutions have been developed for the reversible Selkov model in a reaction-diffusion cell. All the reaction steps have been included in the model so a set of four coupled pdes is obtained, for the concentrations of the reactant, autocatalyst, precursor and final product. It is found that the rate constants, μ_1 and μ_2, associated with the precursor and final products, significantly alter the static and dynamic stability of the system. These parameters affect the shape of the parameter maps for both the bifurcation diagrams and on the regions in which Hopf bifurcations occur. Also, the effect of feedback has been examined, on the Hopf bifurcation regions. Increasing the size of the feedback strength leads to destabilization of the system while decreasing the strength (to negative values of large magnitude) stabilizes the system. Comparisons with numerical solutions show that the two-term semi-analytical model is very accurate. This paper illustrates the accuracy and usefulness of the semi-analytical solution method even for applications

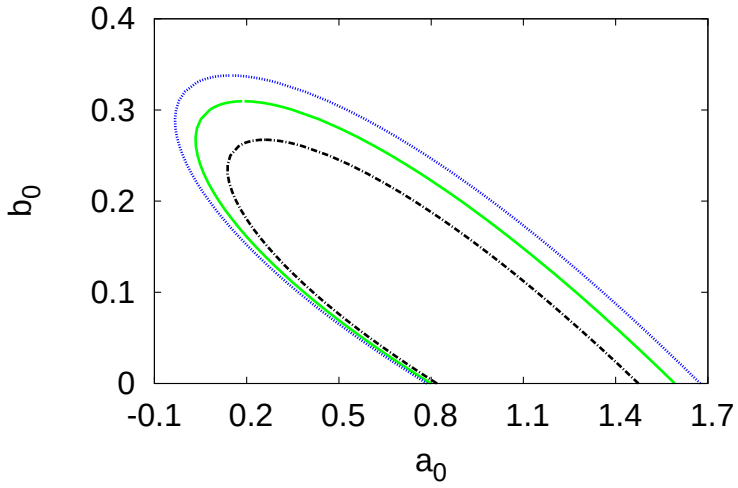

Figure 11: Hopf bifurcation curves in the $a_0 - b_0$ plane. Shown is the two-term semi-analytical solutions with feedback strength $H = 0$ (black dashed line), $H = 0.03$ (green solid line) and $H = 0.05$ (blue small dotted line). The other parameters are $D_1 = D_2 = 0.08$, $\mu_1 = \mu_2 = 0.1$, $s_0 = 4$ and $p_0 = 0.4$.

when many reaction steps and chemical species are modelled and the coupled system of governing equations is large.

Acknowledgement
K. S. Al Noufaey sincerely thanks Taif University in Saudi Arabia for awarding him a PhD scholarship to study at the University of Wollongong, Australia.

References

[1] K. S. Al Noufaey and T. R. Marchant, Semi-analytical solutions for the reversible Selkov model with feedback delay, *Appl. Math. Comput.*, **232** (2014) 49–59.

[2] M. R. Alharthi, T. R. Marchant, and M. I. Nelson, Semi-analytical solutions for cubic autocatalytic reaction-diffusion equations; the effect of a precursor chemical, *ANZIAM J.*, **53** (2012) C511–C524.

[3] V. Balakotaiah and D. Luss, Multiplicity features of reacting systems, *Chem. Engng. Sci.*, **38** (1983) 1709–1721.

[4] J. M. L Corbel, J. N. J. Van Lingen, J. F. Zevenbergen, O. L. J. Gijzeman, and A. Meijerink, Strobes: pyrotechnic compositions that show

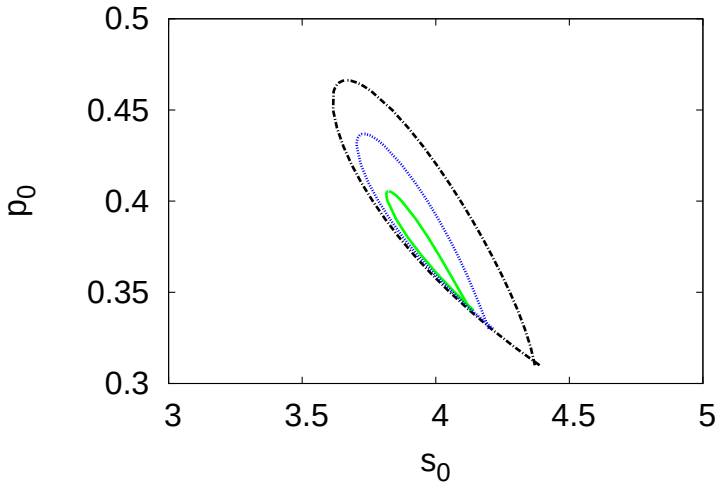

Figure 12: Hopf bifurcation curves in the $s_0 - p_0$ plane. $H = 0$ (black dashed line), $H = -0.05$ (blue small dotted line) and $H = -0.1$ (green solid line). The other parameters are $D_1 = D_2 = 0.08$, $\mu_1 = \mu_2 = 0.1$, $a_0 = 1$ and $b_0 = 0.1$.

a curious oscillatory combustion, *Angew. Chem. Int. Ed.*, **52** (2013) 290–303.

[5] M Dolnik, A. S. Banks, and I. R. Epstein, Oscillatory chemical reaction in a CSTR with feedback control of flow rate, *J. Phys. Chem.*, **101** (1997) 5148–5154.

[6] A. K. Dutt, The effect of diffusion on the Hopf-bifurcation in a model glycolytic reaction exhibiting oscillations, *Chem. Phys. Lett.*, **357** (2002) 341–345.

[7] A. Goldbeter, C. Gerard, D. Gonze, J.C. Leloup, and G. Dupont, Systems biology and cellular rhythms, *FEBS Lett.*, **586** (2012) 2955–2965.

[8] M. Golubitsky and D. G. Schaeffer, Singularites and groups in bifurcation theory, Springer-Verlag, New York, 1985.

[9] J. Guckenheimer and P. Holmes, Nonlinear oscillations, dynamical systems, and bifurcations of vector fields, Springer-Verlag, New York, 1983.

[10] I.Z. Kiss, Z. Kazsu, and V. Gaspar, Tracking unstable steady-states and periodic orbits of oscillatory and chaotic electrochemical systems using delayed feedback control, *Chaos*, **16** (2006) 033109.

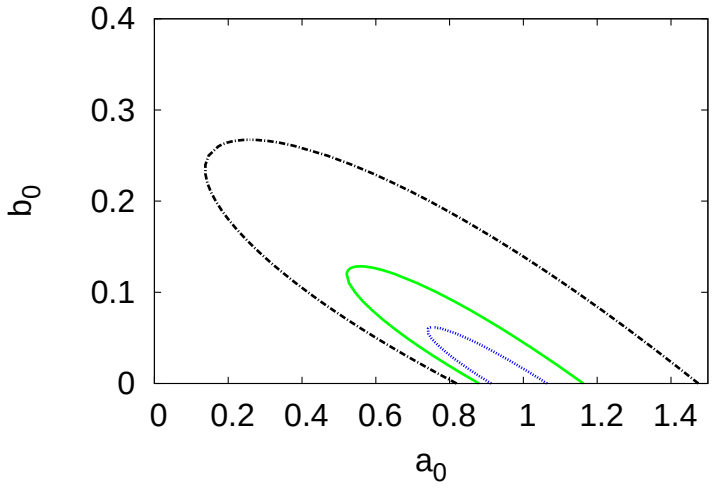

Figure 13: Hopf bifurcation curves in the $a_0 - p_0$ plane. Shown is the two-term semi-analytical solutions with feedback strength $H = 0$ (black dashed line), $H = -0.1$ (green solid line) and $H = -0.15$ (blue small dotted line). The other parameters are $D_1 = D_2 = 0.08$, $\mu_1 = \mu_2 = 0.1$, $s_0 = 4$ and $p_0 = 0.4$.

[11] B. Liu and T. R. Marchant, The occurrence of limit-cycles during feedback control of microwave heating, *Math. Comput. Model.*, **35** (2002) 1095–1118.

[12] T. R. Marchant, Cubic autocatalytic reaction-diffusion equations: semi-analytical solutions, *Proc. Roy. Soc. Lond A*, **458** (2002) 873–888.

[13] T. R. Marchant, Cubic autocatalysis with Michaelis-Menten kinetics: semi-analytical solutions for the reaction-diffusion cell, *Chem. Engng. Sci.*, **59** (2004) 34333440.

[14] T. R. Marchant and M. I. Nelson, Semi-analytical solutions for one and two-dimensional pellet problems, *Proc. Roy. Soc. Lond A*, **460** (2004) 2381–2394.

[15] J. H. Merkin, D. J. Needham, and S. K. Scott, On the creation, growth and extinction of oscillatory solutions for a simple pooled chemical reaction scheme, *SIAM J. Appl. Math.*, **47** (1987) 1040–1060.

[16] K. Miroslav, Delay Compensation for Nonlinear, Adaptive, and PDE Systems, Birkhauser Boston Inc, 2009.

[17] B. Peng, S. K. Scott, and K. Showalter, Transient chaos in a closed chemical system, *J. Cmem. Phys.*, **94** (1991) 1134–1140.

[18] P. Richter, P. Regmus, and J. Ross, Control and dissipation in oscillatory chemical engines, *Prog. Theor. Phys.*, **66** (1981) 385–405.

[19] E. E. Selkov, Self-oscillations in glycolysis, *Eur. J. Biochem.*, **4** (1968) 79–86.

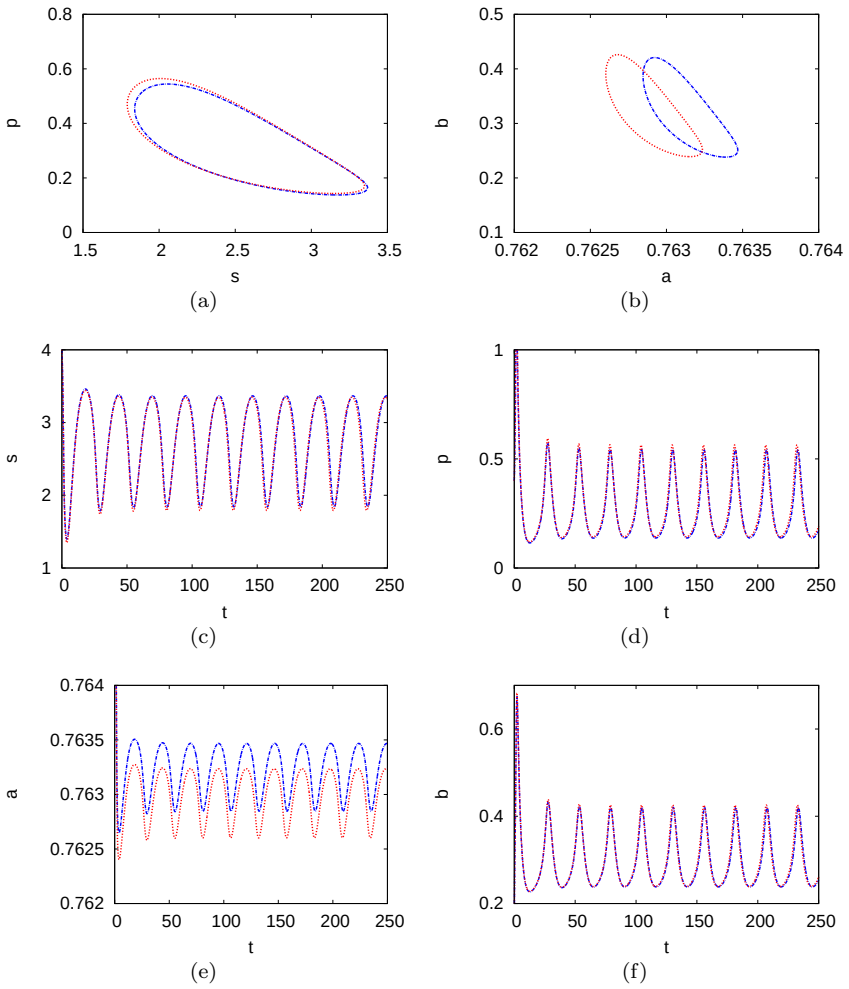

Figure 14: The limit cycle curves s versus p, (a), and a versus b, (b), and the evolution of s, (c), and p, (d), and a, (e), and b, (f), at $x = 0$ versus t. The two-term semi-analytical solution (blue dashed line) and the numerical solution (red dotted line) are shown. The parameters are $s_0 = 4$, $p_0 = 0.4$, $\mu_1 = \mu_2 = 0.1$, $D_1 = D_2 = 0.08$, $a_0 = 0.8$, $b_0 = 0.15$, $H = 0$ and $\kappa = 0.001$.

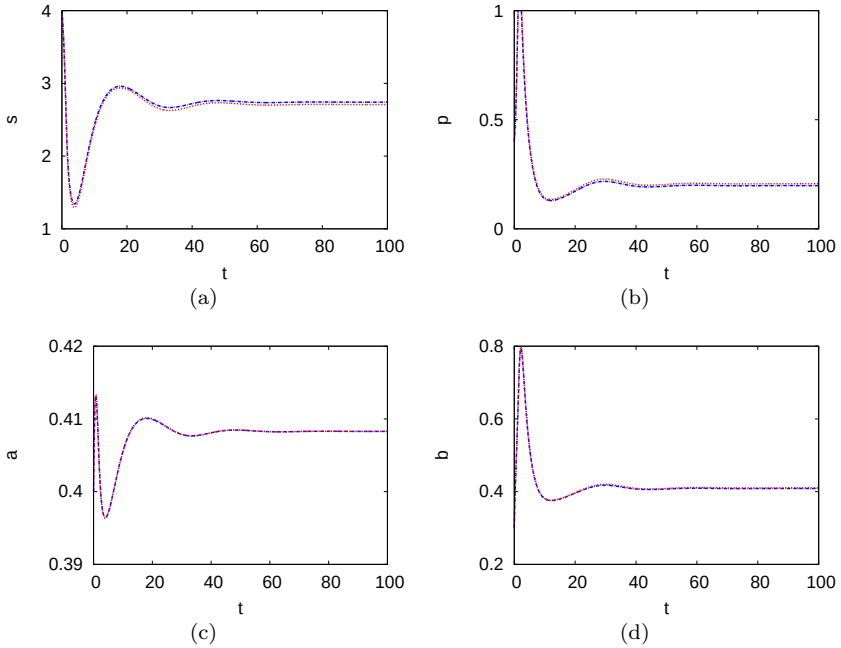

Figure 15: The evolution of s, (a), and p, (b), and a, (c), and b, (d), at $x = 0$ versus t. The two-term semi-analytical solution (blue dashed line) and The numerical solution (red dotted line) are shown. The parameters are $s_0 = 4$, $p_0 = 0.4$, $D_1 = D_2 = 0.08$, $\mu_1 = \mu_2 = 0.1$, $a_0 = 0.4$, $b_0 = 0.3$, $H = 0$ and $\kappa = 0.02$